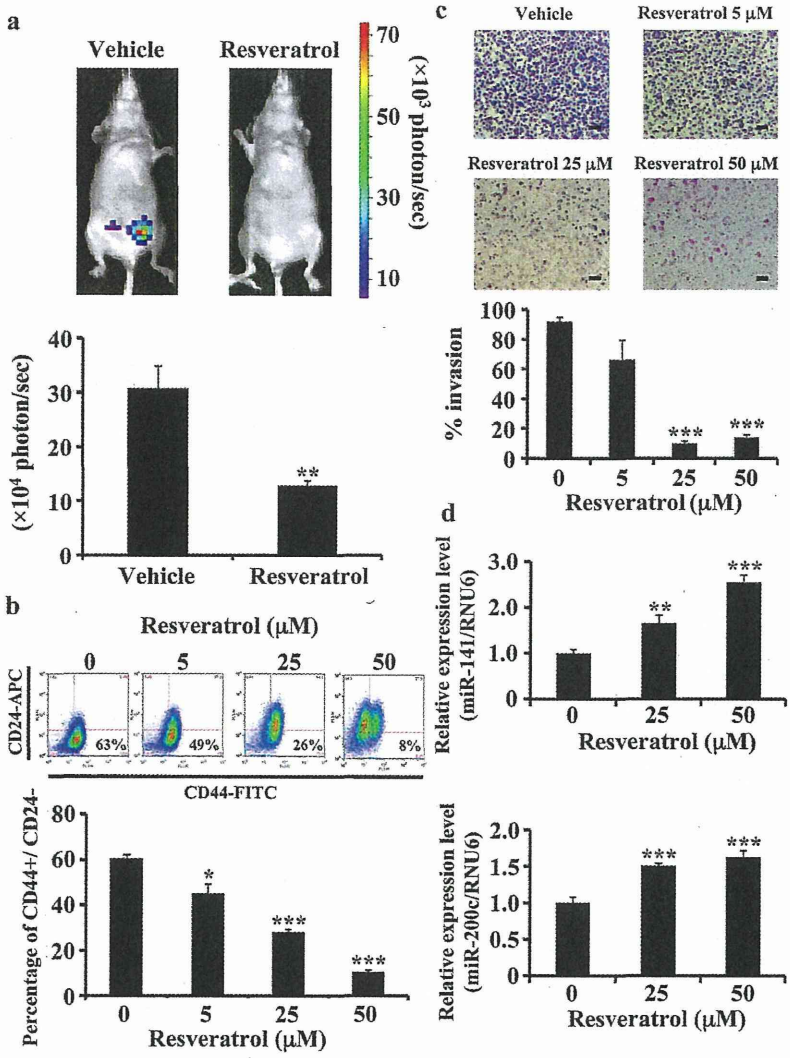

Figure 1 | Multiple anti-cancer effects of resveratrol through the activation of miR-141 and miR-200c. (a) MDA-MB231-luc-D3H2LN cells (200 cells) were injected into the mammary fat pad of six-week-old female SCID hairless outbred mice (n = 5). They were then treated with resveratrol (25 mg/kg/day) by intraperitoneal injection every day for 8 days. Tumour growth was monitored by injecting luciferin in the mice followed by measuring bioluminescence using an IVIS imaging system. Representative mouse images at day 8 (upper panel) and quantified bioluminescence images at day 8 (lower panel) are shown. (b) MDA-MB231-luc-D3H2LN cells were treated with resveratrol or DMSO (control) at the specified doses for 3 days. The percentage of $CD44^+/CD24^-$ cells after compound treatment in independent experiments with MDA-MB231-luc-D3H2LN cell populations is shown. The $CD44^+/CD24^-$ denoting the CSC-enriched fraction. (c) MDA-MB231-luc-D3H2LN cells were grown, treated with resveratrol or DMSO (control) for 1 day, and then subjected to an invasion assay. Representative photographs (upper panel) and quantification (lower panel) are shown. Scale bar: 100 μm. (d) The miR-141 and miR-200c expression levels in MDA-MB231-luc-D3H2LN cells. The expression levels of the indicated miRNAs were examined in MDA-MB231-luc-D3H2LN cells after 48 hour resveratrol treatment (all data are shown as the mean ± s.e.m., *P<0.05, **P<0.01, ***P<0.001).

increased after resveratrol treatment (Supplementary Fig. 6c). In addition, resveratrol induced the luciferase activity of a plasmid containing the Ago2 promoter upstream of the luciferase gene, suggesting that resveratrol transcriptionally induced the expression of Ago2 (Supplementary Fig. 6d). The Ago2 protein is a key regulator of miRNA homeostasis and, upon recognition, it can either cleave or remain tethered to an mRNA to repress its translation and/or regulate its stability[25]. To reveal the relationship between Ago2 and miRNAs, we first quantified the miRNA expression in MDA-MB-231-luc-D3H2LN cells transfected with the Ago2 expression vector. The induction of Ago2 expression by the Ago2 expression vector was confirmed by qRT-PCR (Fig. 2d). After transfection of the Ago2 expression vector, a subset of miRNAs including miR-16, miR-141, miR-143, and miR-200c was higher than in the control cells (Fig. 2e and Supplementary Fig. 6e). To further study the relationship between resveratrol-induced Ago2 and RNAi activity, MDA-MB-231-luc-D3H2LN cells were transfected with luciferase siRNA in the presence of resveratrol treatment and subjected to an *in vitro* firefly luciferase assay. If the induction of Ago2 expression leads to the enhancement of RNAi activity in cells, the luciferase siRNA silencing effect of the luciferase gene in MDA-MB-231-luc-D3H2LN cells may be enhanced after Ago2 over-expression even in the presence of a low siRNA dose and a prolonged period after siRNA transfection. As shown in Fig. 2f, the resveratrol-induced Ago2 resulted in a long-term gene-silencing response in MDA-MB-231-luc-D3H2LN cells. In addition, Ago2 over-expression in HEK293 cells demonstrated a long-term gene-silencing response that was similar to resveratrol-treated MDA-MB-231-luc-D3H2LN cells (Supplementary Fig. 6f).

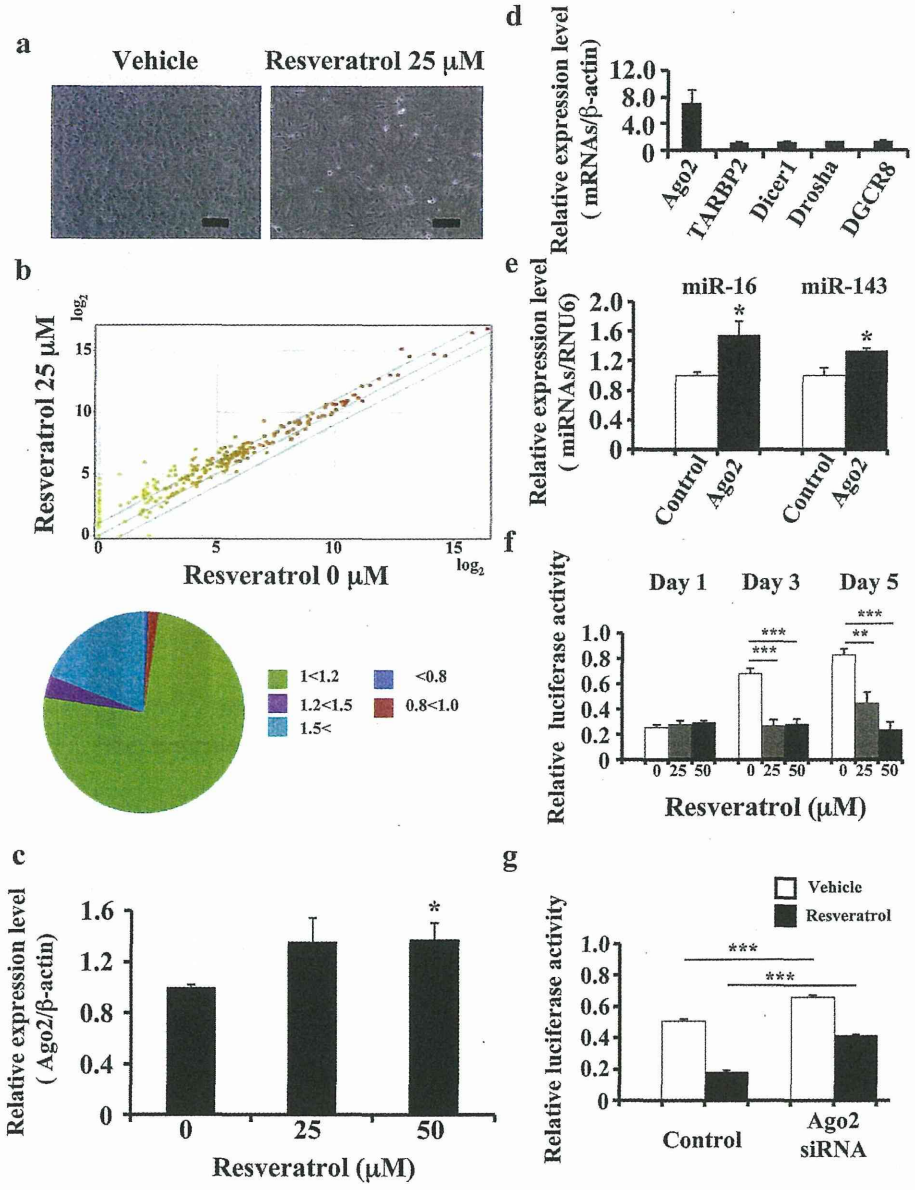

Figure 2 | Association between resveratrol and Ago2. (a) Characteristic microscopic images of MDA-MB231-luc-D3H2LN cells in the presence of DMSO (control) or resveratrol. Scale bar: 100 μm. (b) The effects of resveratrol treatment on miRNA expression in MDA-MB231-luc-D3H2LN cells by miRNA microarray analysis. The proportions of miRNAs at different fold change levels are shown in the lower panel. (c) MDA-MB231-luc-D3H2LN cells were treated with resveratrol or DMSO (control). After 2 days of culture, the cell extract was subjected to real-time mRNA qRT-PCR. (d), (e) MDA-MB231-luc-D3H2LN cells were grown and transiently transfected with Ago2 or EGFP-IRES vector (control). After 2 days of culture, the cell extract was subjected to real-time mRNA (d) and miRNA (e) qRT-PCR. The values on the *y-axis* are depicted relative to the expression level of the EGFP-IRES control vector, which is defined as 1. (f) MDA-MB231-luc-D3H2LN cells were grown and transiently transfected with luciferase siRNA or AllStars negative control siRNA (0.1 nM) under resveratrol treatment. After 1, 3, or 5 days of culture, the cells were subjected to a luciferase reporter assay. The values on the *y-axis* are depicted relative to the luciferase activity of the AllStars Negative Control siRNA, which is defined as 1. (g) MDA-MB231-luc-D3H2LN cells were grown and transiently transfected with luciferase siRNA or AllStars Negative Control siRNA and Ago2 siRNA or AllStars Negative Control siRNA. After 3 days of culture, the cells were subjected to a luciferase reporter assay. The values on the *y-axis* are depicted relative to the luciferase activity of the negative control siRNA, which is defined as 1 (all data are shown as the mean ± s.e.m., *P<0.05, **P<0.01, ***P<0.001).

Moreover, we performed an RNAi experiment to target Ago2 after resveratrol treatment and then assessed the RNAi activity demonstrated by the luciferase siRNA directed against the luciferase gene. The reduction in Ago2 expression by Ago2 siRNA was confirmed by qRT-PCR (Supplementary Fig. 6g). As shown in Fig. 2g, Ago2 siRNA-mediated silencing inhibited the RNAi activity in MDA-MB-231-luc-D3H2LN cells. Taken together, these results indicate that the resveratrol anti-cancer activities were mediated by not only tumour suppressive miRNA upregulation but also by the enhancement of the RNAi activity regulated by Ago2.

Resveratrol-induced miRNA exert an anti-cancer effect. It has been reported that miR-141 inhibits the epithelial-mesenchymal transition and cancer cell migration in breast cancer cells[26]. In addition, we found that resveratrol induced the expression of miR-141 and miR-200c in MDA-MB-231-luc-D3H2LN cells (Fig. 1d). In

Table 1 | A list of miRNAs which were up-regulated more than 2.0-fold by resveratrol in MDA-MB-231-luc-D3H2LN cells compared with control

miRNA	Fold change
Tumor-suppressive miRNA	
hsa-miR-141	4.48
hsa-miR-26a	2.33
hsa-miR-195	3.38
hsa-miR-126	2.41
hsa-miR-185	2.75
hsa-miR-340	11.07
hsa-miR-128	2.13
hsa-miR-34a	2.65
hsa-miR-193b	2.58
hsa-miR-335	2.42
hsa-miR-200c	3.47
hsa-miR-196a	2.67
hsa-miR-497	4.60
hsa-miR-125a-3p	3.00
Onco- miRNA	
hsa-miR-378*	4.81
hsa-miR-10b	5.11
hsa-miR-132	7.23
hsa-miR-222	2.40

contrast, the CSC population was decreased (Fig. 1b). To show direct evidence of whether multiple phenotypes induced by resveratrol were regulated by tumour-suppressive miRNAs, MDA-MB-231-luc-D3H2LN cells were transfected with an antisense oligonucleotide targeting miR-141 (i.e., a miR-141 inhibitor) in the presence of resveratrol treatment. MiR-141 repression by the miR-141 inhibitor was confirmed by qRT-PCR (supplementary Fig. 7a). As shown in Fig. 3a, the miR-141-induced inhibition of invasion was abrogated by the addition of the miR-141 inhibitor, and the MDA-MB-231-luc-D3H2LN cell invasiveness was increased. To confirm the link between resveratrol and miRNA expression, we investigated the growth of breast cancer cells in the presence or absence of a miR-143 inhibitor[27]. In the presence of resveratrol, miR-143-induced inhibition significantly increased the survival of MDA-MB-231-luc-D3H2LN cells relative to the control (Fig. 3b). It has been shown that miR-200c up-regulation in breast cancer cells inhibits Zeb1 expression, resulting in E-cadherin induction in breast cancer cell lines[28]. As shown in Fig. 1d, we found miR-200c up-regulation after resveratrol treatment, suggesting that resveratrol treatment activates this pathway and demonstrating its anti-cancer activity. Indeed, resveratrol addition significantly suppressed Zeb1 expression in the breast cancer cell lines (Fig. 3c) and induced E-cadherin expression in those cells (supplementary Fig. 7b). Furthermore, to show the direct effects of resveratrol on the miRNA machinery, we performed a Zeb1 3′UTR assay and demonstrated that resveratrol treatment significantly down-regulated the luciferase activity of a plasmid containing the Zeb1 3′UTR (Fig. 3d). Taken together, these results suggested that resveratrol plays an important role in breast cancer prevention by up-regulating tumour-suppressive miRNAs.

The stilbene family regulates miRNA biogenesis. The naturally occurring dimethylether resveratrol analogue pterostilbene is a stilbene family member that is generated by plants. Pterostilbene has also been reported to possess chemopreventive activity in cancer and other resveratrol-like health benefits[29,30]. To determine whether pterostilbene induced the expression of tumour-suppressive miRNAs in a similar manner as resveratrol, we assessed the effect of pterostilbene on miRNA expression. As shown in Fig. 4a, pterostilbene treatment suppressed cell growth more significantly than resveratrol treatment in MDA-MB-231-luc-D3H2LN cells. In addition, the expression of tumour suppressive miRNAs (i.e., miR-143 and miR-200c) and Ago2 was significantly higher in pterostilbene-treated MDA-MB-231-luc-D3H2LN cells than in resveratrol-treated cells (Figs. 4b-d and Supplementary Fig. 8). Taken together, these results suggest that resveratrol-induced tumour-suppressive miRNA expression and its anti-cancer activity are conserved among stilbene family members (Fig. 4e).

Discussion

Resveratrol exhibits strong anti-oxidant activity and is capable of inducing apoptosis in cancer cells. Therefore, resveratrol is believed to be efficacious at multiple carcinogenesis stages[4]. However, the underlying molecular mechanism of its anti-tumour activity has yet to be defined. In this study, we demonstrated that resveratrol up-regulated tumour-suppressive miRNAs, resulting in the induction of an anti-cancer effect against the CSC phenotype in cancer cells. We also demonstrated that resveratrol inhibited the invasiveness of breast cancer cells as one of the CSC phenotypes by activating miR-141 and miR-200c. However, the reason why resveratrol reduces the CSC population remains elusive. Recent studies have provided evidence that miR-200c strongly inhibits the ability of breast CSCs to form tumours *in vivo*[31]. These findings suggest that resveratrol shows multiple anti-cancer effects by reducing the CSC population through miR-200c activation.

Argonaute proteins are widely expressed and are involved in post-transcriptional gene silencing. Using microarrays to compare control and $Ago2^{-/-}$ cells, recent studies have demonstrated that Ago2 loss results in the global reduction of mature miRNAs in erythroblasts, fibroblasts, and hepatocytes[32]. However, it has not been determined whether Ago2 alterations can contribute to miRNA expression and the RNAi response. In this study, we show that Ago2 up-regulation by resveratrol leads to an increase in tumour-suppressive miRNAs and the enhancement of RNAi activity.

Pterostilbene has anti-diabetic properties and has been shown to be cytotoxic to a number of cancer cell lines *in vitro*[29,30]. Although pterostilbene and resveratrol have similar pharmacological properties, pterostilbene contains two methoxy groups and one hydroxyl group, while resveratrol has three hydroxyl groups (Supplementary Fig. 9). A recent study demonstrated that pterostilbene shows 95% bioavailability when orally administered, while resveratrol only has 20% bioavailability[33]. Furthermore, pterostilbene is a more powerful chemopreventive agent than resveratrol in colon cancer[34], showing that pterostilbene has several key advantages over resveratrol. In this study, we demonstrate that pterostilbene is more reliable than resveratrol in mediating the anti-cancer effect by inducing tumour-suppressive miRNAs and Ago2 expression. The reason for the difference in the anti-cancer activity of pterostilbene and resveratrol in cancer cells may be due to the expressed miRNAs.

It has been demonstrated that most tumours are characterised by globally diminished miRNA expression[16,17,35]. Thus, the delivery of tumour suppressive miRNAs may allow for the therapeutic restitution of physiological regulation programs lost in cancer and other disease states. However, miRNA therapy shares many of the disadvantages of other treatment approaches including delivery limitations and instability. Therefore, novel methods are required to resolve these issues. Based on this study, we hypothesise that the down-regulation of miRNAs in cancer cells is compensated by resveratrol, which induces the derepression of tumour suppressive miRNAs. Down-regulation of oncogenic miRNAs and up-regulation of tumour-suppressive miRNAs by resveratrol in prostate cancer cells has been reported[36]; however, the connection between resveratrol and the miRNA biogenesis machinery has not been investigated in detail. In this report, we demonstrated that resveratrol leads to a reduction in malignancy by not only activating tumour-suppressive miRNA transcription (Figs. 1d and 2b) but also enhancing the RNAi activity mediated by Ago2 induction (Figs. 2d, e, f and g). Our

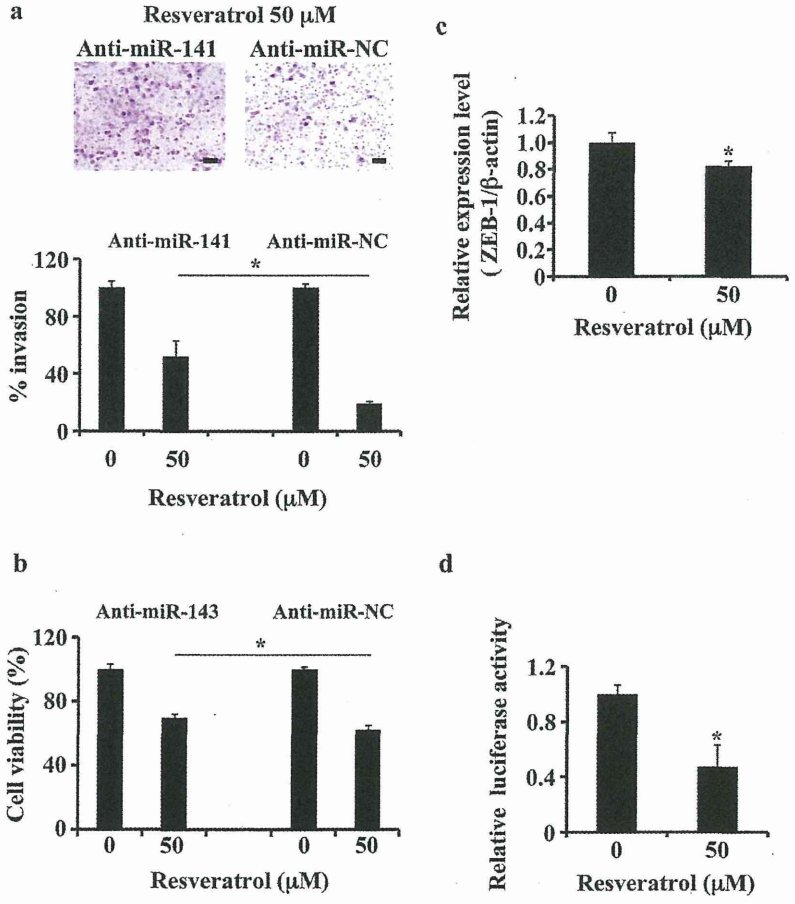

Figure 3 | Multiple anti-cancer effects of tumour-suppressive miRNAs induced by resveratrol. (a) MDA-MB231-luc-D3H2LN cells were grown and transiently transfected with anti-miR-141 or anti-miR-NC (control). After 4 hours, the cells were treated with resveratrol or DMSO (control) for 1 day and subjected to an invasion assay. Representative photographs (upper panel) and quantification (lower panel) are shown. Scale bar: 100 μm. (b) MDA-MB231-luc-D3H2LN cells were cultured and transiently transfected with anti-miR-143 or anti-miR-NC (control). After 4 hours, the cells were treated with resveratrol or DMSO (control) for 72 hours, and the cell viability was measured by the MTS assay. (c) MDA-MB231 cells were treated with resveratrol or DMSO (control). After 2 days of culture, the cell extract was subjected to real-time mRNA qRT-PCR. (d) MDA-MB231 cells were grown and transiently transfected with a ZEB-1 3′UTR or psiCheck2 vector (control) under resveratrol treatment. After 1 day of culture, the cells were subjected to a luciferase reporter assay. The values on the *y-axis* are depicted relative to the luciferase activity of cells treated with DMSO, which is defined as 1 (all data are shown as the mean ± s.e.m., *P<0.05).

demonstration that resveratrol potently suppresses even a severe and multifocal carcinogenesis model in the absence of measurable toxicity provides proof of the principle that miRNA replacement by resveratrol may be a clinically viable anti-cancer therapeutic strategy.

In conclusion, this study shows that an orally available small molecule can safely reduce many of the negative consequences at doses acceptable in humans with an overall improvement in health and survival. Our results raise the possibility that the regulation of tumour-suppressive miRNAs by natural agents could be a novel strategy in the design of combinational approaches using conventional therapies for tumour recurrence prevention and in achieving successful treatment outcomes in patients with cancer.

Methods

Reagents. Trans-resveratrol (98% purity) was purchased from Cayman Chemical, pterostilbene (98% purity) from Tokyo Chemical Industry, cycloheximide solution and 5, 6-dichlorobenzimidazole riboside from sigma, and docetaxel from Sanofi-Aventis. The antibiotic solution (containing 10,000 U/mL penicillin and 10 mg/mL streptomycin), the trypsin-EDTA mixture (containing 0.05% trypsin and EDTA), and FBS (fetal bovine serum) were obtained from Invitrogen. The FITC-conjugated anti-CD44 (clone L178) antibody was obtained from Becton Dickinson, and the APC- conjugated anti-CD24 (clone ML5) antibody, from Biolegend. The duplexes of each small interfering RNA (siRNA), targeting human Ago2 mRNA (siAgo2-1, GCACGGAAGUCCAUCUGAAUU, UUCAGAUGGACUUCCGUGCUU; siAgo2-2, GCAGGACAAAGAUGUAUUAUU, UAAUACAUCUUUGUCCUGCUU; siAgo2-3, GGGUCUGUGGUGAUAAAUAUU, UAUUUAUCACCACAGACCCUU; siAgo2-4, GUAUGAGAACCCAAUGUCAUU, UGACAUUGGGUUCUCAUACUU) and negative control 1 were purchased from Applied Biosystems[37].

Plasmids. The primary-miR-143 expression vector was purchased from TaKaRa BIO. The full-length human Ago2 cDNA was cloned into pIRES2-EGFP vector (Clontech). We amplified the upstream of human Ago2 gene (−1,770/−1 relative to the TSS) by PCR using human genomic DNA as template, and we cloned it into the pGL3-Basic vector. For the 3′UTR reporter plasmids, the nucleotides +3,399 to +3,953 of human ZEB1 cDNA were amplified and cloned downstream of the luciferase gene in the psiCHECK2 vector (Promega). For cloning the following primers were used for PCR: Ago2 promoter: 5′-ACGCGTATAGGGGATATGTGAAGGAGACA-3′ (forward) and 5′-CTCGAGATA CGCGCGCGCCACGGGCCCCG-3′ (reverse); ZEB1 3′UTR Fragment: 5′-ATAATACGCGTTAAAGGAAGCTGATTAATTAGATATGC-3′ (forward) and 5′-ATAATAAGCTTTTTGTAGTGCAGAAGTTCTCACATTTT-3′ (reverse)[22].

Cell culture. HEK293 cells (American Type Culture Collection) were cultured in Dulbecco's Modified Eagle's Medium containing 10% heat-inactivated FBS and an antibiotic-antimycotic (Invitrogen) at 37°C in 5% CO_2. MDA-MB-231 cells (American Type Culture Collection) and MDA-MB-231-luc-D3H2LN cells (Xenogen) were cultured in RPMI containing 10% heat-inactivated FBS and antibiotic-antimycotic at 37°C in 5% CO_2. Human mammary carcinoma cell lines, MCF7 cells and multidrug-resistant MCF7-ADR cells were provided by Shien-Lab,

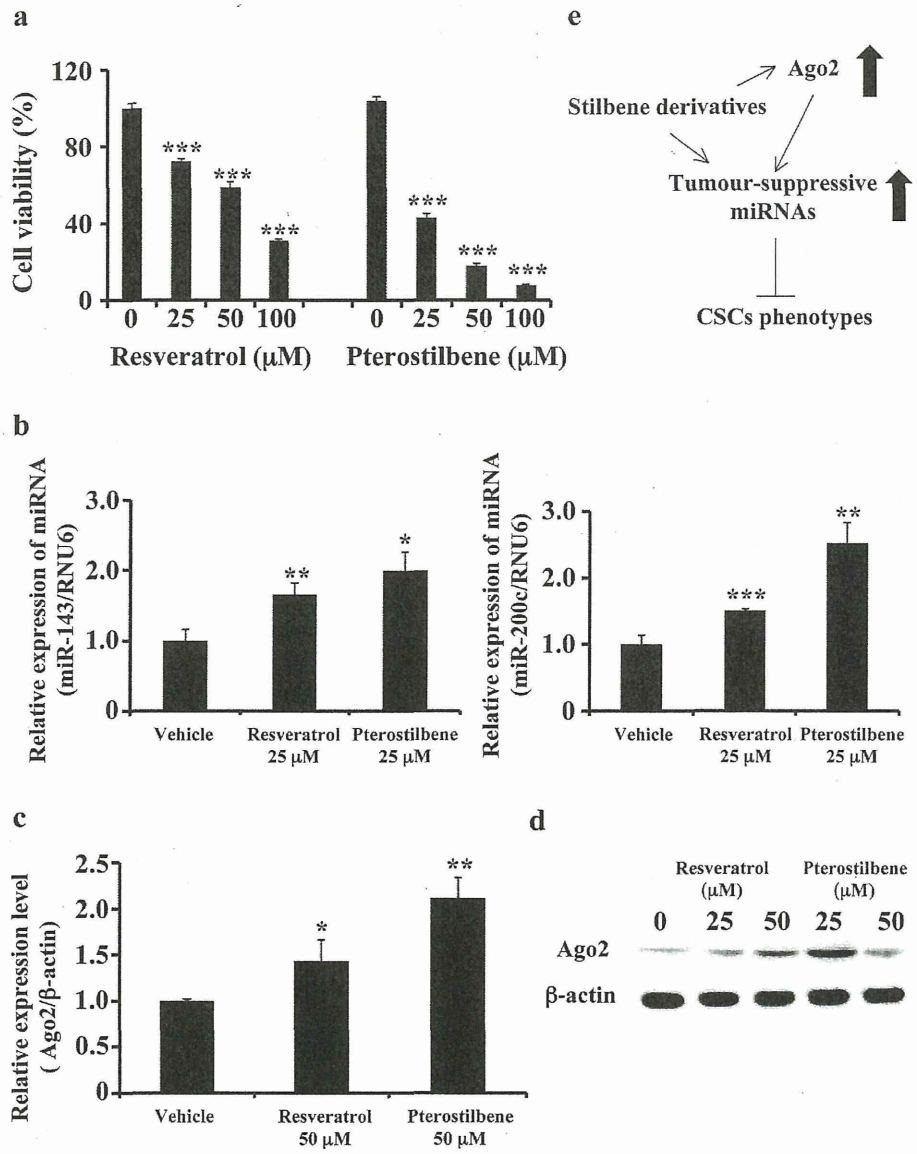

Figure 4 | Effects of pterostilbene on human breast cancer cells. (a) MDA-MB231-luc-D3H2LN cells were cultured in the presence or absence of resveratrol or pterostilbene at the indicated concentrations for 72 hours. Cell viability was measured using the MTS assay. The control wells were treated with DMSO. (b), (c) Expression levels of miR-143, miR-200c (b), and Ago2 (c) in MDA-MB231-luc-D3H2LN cells. The expression levels of the indicated miRNAs were examined in MDA-MB231-luc-D3H2LN cells 48 hours after treatment with pterostilbene. (d) MDA-MB231-luc-D3H2LN cells were treated with stilbenes for 72 hours, and Ago2 expression was detected by immunoblotting. Actin was used as a loading control. (e) Model of the regulation of tumour-suppressive miRNAs and Ago2 expression in the stilbene family (all data are shown as the mean ± s.e.m., *$P<0.05$, **$P<0.01$, ***$P<0.001$).

Medical Oncology, National Cancer Center Hospital of Japan. These cells were maintained in RPMI supplemented with 10% heat-inactivated FBS and antibiotic-antimycotic at 37°C in 5% CO_2. MCF10A cells, which were a spontaneously immortalized nontumorigenic epithelial cell line, (American Type Culture Collection) were maintained in an MEBM medium with 1% GA-1000, 50 μg/ml hydrocortisone, 1 μg/ml hEGF, 500 μg/ml insulin, and 4% BPE (Lonza) at 37°C in 5% CO_2.

Cell proliferation assay (MTS assay). Five thousand cells per well were seeded in 96-well plates. The following day, the cells were treated with resveratrol. After 3 days of culture, cell viability was measured using the Tetra Color One assay kit (Seikagaku Kohgyo) according to the instructions of the manufacturer. The absorbance at 450 nm was measured using Envision (Wallac).

Transwell invasion assay. Breast cancer cell invasion was assayed in 24-well Biocoat Matrigel invasion chambers (8 μm; Becton Dickinson) according to the manufacturer's protocol. Briefly, the cells were treated with resveratrol, and on the following day, 20,000 cells were plated in the upper chamber. The upper chamber contained resveratrol and the bottom chamber contained 10% FBS as a chemoattractant. Twenty-two hours later, the non-invasive cells were removed with a cotton swab. The cells that migrated through the membrane and stuck to the lower surface of the membrane were fixed with methanol and stained with Diff Quick staining. For quantification, the cells were counted under a microscope in four random fields. All assays were performed in triplicate. The data are expressed as the invasion percentage through the Matrigel matrix and membrane relative to migration through the control membrane according to the manufacturer's instructions.

Cell growth inhibition by cytotoxic agents and resveratrol. Breast cancer cells were plated as described above and allowed to attach overnight. The cultures were replenished with fresh medium containing 25 μM resveratrol for 24 hours and then exposed to 2.5 nM of the chemotherapeutic agent docetaxel for an additional 48 hours. Thus, for a single-agent treatment, the cells were exposed to resveratrol or docetaxel for 72 hours. The effect of resveratrol pretreatment on cell viability was examined by the MTS assay method.

Cell sorting and flow cytometric analysis. MDA-MB-231-luc-D3H2LN cells were treated with resveratrol. After culturing for 3 days, MDA-MB-231-luc-D3H2LN cells were suspended in their culture medium and subjected to a JSAN cell sorter (Bay Bioscience). At least one million cells were pelleted by centrifugation at 180 x *g* for 5 minutes at 4°C, resuspended in a 5-μL mixture of a monoclonal mouse anti-human CD44-FITC antibody (Becton Dickinson, clone L178) and a monoclonal mouse anti-human CD24-APC antibody (Biolegend, clone ML5), and incubated for 30 minutes at 4°C. Three independent experiments were performed.

Mammosphere assay. The CD44+/CD24− fraction from MDA-MB-231-luc-D3H2LN cells were resuspended in 1 : 1 DMEM/F12 (Invitrogen) basal medium freshly supplemented with 20 ng/mL human basic fibroblast growth factor (Invitrogen), 20 ng/mL epidermal growth factor (Invitrogen), 10 μg/mL heparin (Sigma-Aldrich), and 1 : 50 B27 supplement without vitamin A (Sigma-Aldrich) and seeded in 10-cm Ultra-Low Attachment Surface plates (Corning) at a density of 5000 cells. Ten days later, the plates were analysed for mammosphere formation.

Tumourigenicity assays in SCID hairless outbred mice. Six-week-old female SCID hairless outbred (SHO) mice were subcutaneously injected with 200 MDA-MB231-luc-D3H2LN cells in 25 μL of PBS and 25 μL of matrigel (n = 5). The mice were then treated with resveratrol (25 mg/kg/day) or ethanol (control) by intraperitoneal injection every day for 8 days. The tumour growth was monitored by injecting luciferin in the mice followed by measuring bioluminescence using an IVIS imaging system. The data were analysed using the LIVINGIMAGE 2.50 software (Xenogen). Six-week-old female SCID Hairless Outbred (SHO) mice were subcutaneously injected with 2000 MDA-MB231-luc-D3H2LN cells in 25 μL of PBS and 25 μL of Matrigel (n = 5). The mice were then treated with resveratrol (25 mg/kg) by intraperitoneal injection (IP) every day for 2 weeks and then with docetaxel (20 mg/kg) by intraperitoneal injection (IP) once per week for 2 weeks. The normalised fold changes (day 22 or day 29/day 15) of bioluminescence emitted from the whole body of the mice are shown. All experimental protocols involving animals were approved by the the Institute for Laboratory Animal Research, National Cancer Center Research Institute.

Isolation of microRNAs. Total RNAs were extracted from cultured cells using the QIAzol and miRNeasy Mini Kit (Qiagen) according to the manufacturer's protocol.

Quantitative Real-Time PCR (qRT-PCR). The qRT-PCR method has been previously described[38]. PCR was performed in 96-well plates using the 7300 Real-Time PCR System (Applied Biosystems). All reactions were performed in triplicate. All of the TaqMan microRNA assays were purchased from Applied Biosystems. hRNU6 was used as an invariant control. SYBR Green I qRT-PCR was performed, and the β-actin housekeeping gene was used to normalise the variation in the cDNA levels. The following pairs of primers were used for gene amplification: for pri-miR-16, 5′-GCAATTACAGTATTTTAAGAGATGAT-3′ (forward) and 5′- CAT-ACTCTACAGTTGTGTTTTAATGT-3′ (reverse); for pri-miR-141-200c, 5′-TGAGCTTGGGACTGCAGAG-3′ (forward) and 5′-CTGAGCCACCTTCCCC-TAC-3′ (reverse); for pri-miR-143, 5′-CAAGGTTTGGTCCTGGGTGCTCAAA-3′ (forward) and 5′-TGGTGGCCTGTGGCGGGACTCCAA-3′ (reverse); for ZEB1, 5′-AAGAATTCACAGTGGAGAGAAGCCA-3′ (forward) and 5′-CGTTTCTTGC-AGTTTGGGCATT-3′ (reverse); for E-cadherin, 5′-GTCCTGGGCAG-ACTGAATTT-3′ (forward) and 5′-GACCAAGAAATGGATCTGTGG-3′ (reverse); and for β-actin, 5′-GGCACCACCATGTACCCTG-3′ (forward) and 5′-CACGG-AGTACTTGCGCTCAG-3′ (reverse)[39].

Quantification of the Ago2 mRNA half-life. MDA-MB231-luc-D3H2LN cells were incubated with 5,6-dichlorobenzimidazole riboside (50 μM), which is an inhibitor of mRNA synthesis. The cells were then treated with 50 μM resveratrol and harvested at the indicated time points. Total cellular RNA was isolated using the RNeasy Mini kit (Qiagen). qRT-PCR analysis of Ago2 mRNA at each time point was performed as described above. The fold-change in the Ago2 mRNA abundance at each time point was determined by the following equation:

Fold change = $2^{-\Delta CT}$, where ΔCT = (CT, Ago2) target - (CT, Ago2) 0 h.

Transient transfection assays. The plasmid transfections were performed using Lipofectamine LTX (Invitrogen). The cell numbers and amount of plasmids for each transfection were determined according to the manufacturer's protocol. The transfection of siRNA and miRNA inhibitors was accomplished using the DharmaFECT transfection reagent (Thermo Scientific) according to the manufacturer's protocol.

Luciferase reporter assay. Cells were seeded in 96-well plates at 3000 cells per well the day before transfection. A total of 500 ng of Ago2 vector, 10 nM siRNA against luciferase and the AllStars negative control were added to each well. The cells were collected 1, 3, or 5 days after transfection and analysed using the Bright-Glo Luciferase Reporter Assay System (Promega).

Immunoblot analysis. SDS-PAGE gels were calibrated using Precision Plus protein standards (161-0375) (Bio-Rad), and anti-Ago2 (1 : 200) and anti-actin (1 : 1,000) were used as the primary antibodies. The dilution ratio of each antibody is indicated in parentheses. A peroxidase-labelled anti-mouse secondary antibody was used at a dilution of 1 : 10,000. Bound antibodies were visualised by chemiluminescence using the ECL Plus Western blotting detection system (RPN2132) (GE HealthCare), and luminescent images were analysed using a LuminoImager (LAS-3000; Fuji Film Inc.).

Quantification of Ago2 protein half-life. MDA-MB-231-luc-D3H2LN cells at 80% confluency were treated with 30 μg/ml cycloheximide (Sigma-Aldrich). The cells were then treated with 50 μM resveratrol and harvested at the indicated time points. The effect of resveratrol on Ago2 stability was examined by immunoblotting as reported above.

Statistical analysis. The data presented in bar graphs are the means ± s.e.m. of at least three independent experiments. Statistical analyses were performed using the Student's t-test.

1. Hartwell, J. L. & Schrecker, A. W. Components of Podophyllin. V. The Constitution of Podophyllotoxin1. *J Am Chem Soc* **73**, 2909–2916 (1951).
2. Baur, J. A. & Sinclair, D. A. Therapeutic potential of resveratrol: the in vivo evidence. *Nat Rev Drug Discov* **5**, 493–506 (2006).
3. Renaud, S. & de Lorgeril, M. Wine, alcohol, platelets, and the French paradox for coronary heart disease. *Lancet* **339**, 1523–1526 (1992).
4. Jang, M. *et al.* Cancer chemopreventive activity of resveratrol, a natural product derived from grapes. *Science* **275**, 218–220 (1997).
5. Fremont, L. Biological effects of resveratrol. *Life Sci* **66**, 663–673 (2000).
6. Hammell, C. M., Lubin, I., Boag, P. R., Blackwell, T. K. & Ambros, V. nhl-2 Modulates microRNA activity in Caenorhabditis elegans. *Cell* **136**, 926–938 (2009).
7. Stefani, G. & Slack, F. J. Small non-coding RNAs in animal development. *Nat Rev Mol Cell Biol* **9**, 219–230 (2008).
8. Kong, D. *et al.* miR-200 regulates PDGF-D-mediated epithelial-mesenchymal transition, adhesion, and invasion of prostate cancer cells. *Stem Cells* **27**, 1712–1721 (2009).
9. Zhao, J. J. *et al.* MicroRNA-221/222 negatively regulates estrogen receptor alpha and is associated with tamoxifen resistance in breast cancer. *J Biol Chem* **283**, 31079–31086 (2008).
10. Takeshita, F. *et al.* Systemic delivery of synthetic microRNA-16 inhibits the growth of metastatic prostate tumors via downregulation of multiple cell-cycle genes. *Mol Ther* **18**, 181–187 (2010).
11. Melkamu, T., Zhang, X., Tan, J., Zeng, Y. & Kassie, F. Alteration of microRNA expression in vinyl carbamate-induced mouse lung tumors and modulation by the chemopreventive agent indole-3-carbinol. *Carcinogenesis* **31**, 252–258 (2010).
12. Tsang, W. P. & Kwok, T. T. Epigallocatechin gallate up-regulation of miR-16 and induction of apoptosis in human cancer cells. *J Nutr Biochem* **21**, 140–146 (2010).
13. Li, Y. *et al.* Up-regulation of miR-200 and let-7 by natural agents leads to the reversal of epithelial-to-mesenchymal transition in gemcitabine-resistant pancreatic cancer cells. *Cancer Res* **69**, 6704–6712 (2009).
14. Sun, M. *et al.* Curcumin (diferuloylmethane) alters the expression profiles of microRNAs in human pancreatic cancer cells. *Mol Cancer Ther* **7**, 464–473 (2008).
15. Lee, H. P. *et al.* Dietary effects on breast-cancer risk in Singapore. *Lancet* **337**, 1197–1200 (1991).
16. Croce, C. M. Causes and consequences of microRNA dysregulation in cancer. *Nat Rev Genet* **10**, 704–714 (2009).
17. Gaur, A. *et al.* Characterization of microRNA expression levels and their biological correlates in human cancer cell lines. *Cancer Res* **67**, 2456–2468 (2007).
18. Al-Hajj, M., Wicha, M. S., Benito-Hernandez, A., Morrison, S. J. & Clarke, M. F. Prospective identification of tumorigenic breast cancer cells. *Proc Natl Acad Sci U S A* **100**, 3983–3988 (2003).
19. Al-Hajj, M. Cancer stem cells and oncology therapeutics. *Curr Opin Oncol* **19**, 61–64 (2007).
20. Al-Hajj, M., Becker, M. W., Wicha, M., Weissman, I. & Clarke, M. F. Therapeutic implications of cancer stem cells. *Curr Opin Genet Dev* **14**, 43–47 (2004).
21. Iorio, M. V. *et al.* MicroRNA gene expression deregulation in human breast cancer. *Cancer Res* **65**, 7065–7070 (2005).
22. Burk, U. *et al.* A reciprocal repression between ZEB1 and members of the miR-200 family promotes EMT and invasion in cancer cells. *EMBO Rep* **9**, 582–589 (2008).
23. Carmell, M. A. & Hannon, G. J. RNase III enzymes and the initiation of gene silencing. *Nat Struct Mol Biol* **11**, 214–218 (2004).
24. Kim, V. N. MicroRNA biogenesis: coordinated cropping and dicing. *Nat Rev Mol Cell Biol* **6**, 376–385 (2005).
25. Lingel, A., Simon, B., Izaurralde, E. & Sattler, M. Structure and nucleic-acid binding of the Drosophila Argonaute 2 PAZ domain. *Nature* **426**, 465–469 (2003).
26. Korpal, M., Lee, E. S., Hu, G. & Kang, Y. The miR-200 family inhibits epithelial-mesenchymal transition and cancer cell migration by direct targeting of E-cadherin transcriptional repressors ZEB1 and ZEB2. *J Biol Chem* **283**, 14910–14914 (2008).
27. Xu, B. *et al.* miR-143 decreases prostate cancer cells proliferation and migration and enhances their sensitivity to docetaxel through suppression of KRAS. *Mol Cell Biochem* **350**, 207–213 (2011).
28. Burk, U. *et al.* A reciprocal repression between ZEB1 and members of the miR-200 family promotes EMT and invasion in cancer cells. *Embo Reports* **9**, 582–589 (2008).

29. Rimando, A. M. *et al.* Cancer chemopreventive and antioxidant activities of pterostilbene, a naturally occurring analogue of resveratrol. *J Agric Food Chem* **50**, 3453–3457 (2002).
30. Stivala, L. A. *et al.* Specific structural determinants are responsible for the antioxidant activity and the cell cycle effects of resveratrol. *J Biol Chem* **276**, 22586–22594 (2001).
31. Shimono, Y. *et al.* Downregulation of miRNA-200c links breast cancer stem cells with normal stem cells. *Cell* **138**, 592–603 (2009).
32. O'Carroll, D. *et al.* A Slicer-independent role for Argonaute 2 in hematopoiesis and the microRNA pathway. *Genes Dev* **21**, 1999–2004 (2007).
33. Kapetanovic, I. M., Muzzio, M., Huang, Z., Thompson, T. N. & McCormick, D. L. Pharmacokinetics, oral bioavailability, and metabolic profile of resveratrol and its dimethylether analog, pterostilbene, in rats. *Cancer Chemother Pharmacol* (2010).
34. Chiou, Y. S. *et al.* Pterostilbene is more potent than resveratrol in preventing azoxymethane (AOM)-induced colon tumorigenesis via activation of the NF-E2-related factor 2 (Nrf2)-mediated antioxidant signaling pathway. *J Agric Food Chem* **59**, 2725–2733 (2011).
35. Chang, T. C. *et al.* Transactivation of miR-34a by p53 broadly influences gene expression and promotes apoptosis. *Mol Cell* **26**, 745–752 (2007).
36. Dhar, S., Hicks, C. & Levenson, A. S. Resveratrol and prostate cancer: Promising role for microRNAs. *Mol Nutr Food Res* **55**, 1219–1229 (2011).
37. Meister, G. *et al.* Human Argonaute2 mediates RNA cleavage targeted by miRNAs and siRNAs. *Mol Cell* **15**, 185–197 (2004).
38. Mitchell, P. S. *et al.* Circulating microRNAs as stable blood-based markers for cancer detection. *Proc Natl Acad Sci U S A* **105**, 10513–10518 (2008).
39. Suzuki, H. I. *et al.* Modulation of microRNA processing by p53. *Nature* **460**, 529–533 (2009).

Acknowledgements

This work was supported in part by a Grant-in-Aid for the Third-Term Comprehensive 10-Year Strategy for Cancer Control, a Grant-in-Aid for Scientific Research on Priority Areas Cancer from the Ministry of Education, Culture, Sports, Science and Technology, the National Cancer Center Research and Development Fund, the Program for Promotion of Fundamental Studies in Health Sciences of the National Institute of Biomedical Innovation (NiBio), Project for Development of Innovative Research on Cancer Therapeutics, and the Japan Society for the Promotion of Science (JSPS) through the "Funding Program for World-Leading Innovative R&D on Science and Technology (FIRST Program)" initiated by the Council for Science and Technology Policy (CSTP). We thank Ayako Inoue for excellent technical assistance. We thank Dr.Izuho Hatada for providing the information about Ago2 promoter region.

Author contributions

TO supervised the project. KH performed a significant amount of the experimental work. TO, KH, NK, and YY wrote the manuscript and prepared the figures and tables. *In vivo* experiments were carried out by KH, NK, YY, RT, and FT.

Additional information

Supplementary information accompanies this paper at http://www.nature.com/scientificreports

Competing financial interests: The authors declare no competing financial interests.

License: This work is licensed under a Creative Commons Attribution-NonCommercial-ShareAlike 3.0 Unported License. To view a copy of this license, visit http://creativecommons.org/licenses/by-nc-sa/3.0/

How to cite this article: Hagiwara, K. *et al.* Stilbene derivatives promote Ago2-dependent tumour-suppressive microRNA activity. *Sci. Rep.* **2**, 314; DOI:10.1038/srep00314 (2012).

Development/Plasticity/Repair

Bcl11b/Ctip2 Controls the Differentiation of Vomeronasal Sensory Neurons in Mice

Takayuki Enomoto,[1] Makoto Ohmoto,[3] Tetsuo Iwata,[1] Ayako Uno,[1] Masato Saitou,[1] Tatsuya Yamaguchi,[1] Ryo Kominami,[4] Ichiro Matsumoto,[3,5] and Junji Hirota[1,2]

[1]Department of Bioengineering, Graduate School of Bioscience and Bioengineering, and [2]Center for Biological Resources and Informatics, Tokyo Institute of Technology, Yokohama 226-8501, Japan, [3]Department of Applied Biological Chemistry, Graduate School of Agricultural and Life Sciences, The University of Tokyo, Tokyo 113-8657, Japan, [4]Department of Molecular Genetics, Graduate School of Medical and Dental Sciences, Niigata University, Niigata 951-8122, Japan, and [5]Monell Chemical Senses Center, Philadelphia, Pennsylvania 19104-3308

The transcription factor Bcl11b/Ctip2 plays critical roles in the development of several systems and organs, including the immune system, CNS, skin, and teeth. Here, we show that *Bcl11b/Ctip2* is highly expressed in the developing vomeronasal system in mice and is required for its proper development. *Bcl11b/Ctip2* is expressed in postmitotic vomeronasal sensory neurons (VSNs) in the vomeronasal epithelium (VNE) as well as projection neurons and GABAergic interneurons in the accessory olfactory bulb (AOB). In the absence of *Bcl11b*, these neurons are born in the correct number, but VSNs selectively die by apoptosis. The critical role of Bcl11b in vomeronasal system development is demonstrated by the abnormal phenotypes of *Bcl11b*-deficient mice: disorganization of layer formation of the AOB, impaired axonal projections of VSNs, a significant reduction in the expression of vomeronasal receptor genes, and defective mature differentiation of VSNs. VSNs can be classified into two major types of neurons, vomeronasal 1 receptor (V1r)/Gα_{i2}-positive and vomeronasal 2 receptor (V2r)/Gα_o-positive VSNs. We found that all Gα_{i2}-positive cells coexpressed Gα_o during embryogenesis. This coexpression is also observed in newly differentiated neurons in the adult VNE. Interestingly, loss of Bcl11b function resulted in an increased number of V1r/Gα_{i2}-type VSNs and a decreased number of V2r/Gα_o-type VSNs, suggesting that Bcl11b regulates the fate choice between these two VSN types. These results indicate that Bcl11b/Ctip2 is an essential regulator of the differentiation and dichotomy of VSNs.

Introduction

Most terrestrial vertebrates possess a vomeronasal system, which detects pheromones to mediate social and reproductive behaviors (Keverne, 1999; Dulac and Torello, 2003; Halpern and Martínez-Marcos, 2003; Brennan and Zufall, 2006). In the mouse, pheromone signals are detected by the vomeronasal sensory neurons (VSNs), which generally express vomeronasal receptor (VR) genes that encode a putative seven-transmembrane domain protein (Dulac and Axel, 1995; Herrada and Dulac, 1997; Matsunami and Buck, 1997; Ryba and Tirindelli, 1997). There are two classic types of VSN, which are distinguished by the location of the cell body within the vomeronasal epithelium (VNE), the class of VR expressed, the type of G-protein subunit expressed, and their axonal target site in the accessory olfactory bulb (AOB). VSNs located apically in the VNE coexpress vomeronasal 1 receptor (V1r) genes along with Gα_{i2} and project their axons to the anterior half of the AOB. In contrast, basally located VSNs coexpress vomeronasal 2 receptor (V2r) genes along with Gα_o and project their axons to the posterior half of the AOB (Berghard and Buck, 1996; Jia and Halpern, 1996). The cell bodies of V1r/Gα_{i2}-positive and V2r/Gα_o-positive VSNs form nonoverlapping layers in the VNE. Although both types of VSNs are generated from Mash1-positive progenitor cells (Murray et al., 2003), the genetic mechanisms that regulate the differentiation and dichotomy of VSNs are not well understood; only a few critical transcription factors are known to regulate the development of VSNs (Murray et al., 2003; Ikeda et al., 2007; Duggan et al., 2008).

The *Bcl11b* gene (also known as *Ctip2* or *Rit1*) encodes a C2H2 zinc finger transcription factor that is predominantly expressed in the immune system, CNS, and the embryonic olfactory system in mice (Avram et al., 2000; Wakabayashi et al., 2003a; Leid et al., 2004). Several studies of *Bcl11b*-deficient (*Bcl11b*$^{-/-}$) mice have demonstrated that Bcl11b is required for T-cell development, the axonal projections of corticospinal motor neurons, the differentiation of medium spiny neurons of the striatum, skin morphogenesis, and odontogenesis (Wakabayashi et al., 2003b; Arlotta et al., 2005, 2008; Albu et al., 2007; Golonzhka et al., 2009a,b; Ikawa et al., 2010; Li et al., 2010a,b). In this study, we investigated the expression and function of *Bcl11b* in the developing vomeronasal system *in vivo*. We found that the expression of *Bcl11b* changed

Received March 10, 2011; revised May 26, 2011; accepted May 26, 2011.

Author contributions: J.H. designed research; T.E., M.O., T.I., A.U., M.S., T.Y., and J.H. performed research; R.K. and I.M. contributed unpublished reagents/analytic tools; T.E., M.O., and J.H. analyzed data; T.E. and J.H. wrote the paper.

This work was supported in part by the Ministry of Education, Culture, Sports, Science and Technology of Japan, Grant-in-Aid for Young Scientists (B) to M.O, Grant-in-Aid for Young Scientists (A) to I.M., and Grants-in-Aid for Scientific Research (C) to J.H.; by the National Institute on Deafness and Other Communication Disorders (Grant R03 DC011143) to I.M.; by the Japan Society for the Promotion of Science, Grant-in-Aid for Scientific Research on Innovative Areas to J.H.; and by grants from the Senri Life Science Foundation, the Inamori Foundation, and the Sumitomo Foundation to J.H. We thank Drs. P. Mombaerts and Y. Yoshihara for providing reagents, Dr. S. Fuss for instructions on the DiI experiment and critical review of the manuscript, and the members of the Hirota laboratory for their continuous support.

Correspondence should be addressed to Junji Hirota at the above address. E-mail: jhirota@bio.titech.ac.jp.

DOI:10.1523/JNEUROSCI.1245-11.2011

Copyright © 2011 the authors 0270-6474/11/3110159-15$15.00/0

dynamically during the development of the VNE and AOB from embryogenesis to adulthood. The loss of function of Bcl11b resulted in severe abnormalities in the vomeronasal system, including the disorganization of layer formation in the AOB, impaired axonal projection of VSNs, a severe reduction of *VR* gene expression, defects in mature differentiation of VSNs, and distinct changes in the expression of several genes in VSNs. In addition, a deficiency of Bcl11b disturbs the balance between the two types of VSNs produced, suggesting that Bcl11b regulates the fate choice between these cell types, indicating that Bcl11b is a critical regulator during functional development of the vomeronasal system.

Materials and Methods

Mutant mice. *Bcl11b*$^{-/-}$ and *Mash1*$^{-/-}$ mice were generated as described previously(Guillemot et al., 1993; Wakabayashi et al., 2003b). Mutant and wild-type mice/embryos of either sex were used. For embryo staging, mid-day of the day of the vaginal plug was designated as embryonic day (E) 0.5. The day of birth was designated postnatal day (P) 0. All mouse studies were approved by the Institutional Animal Experiment Committee of the Tokyo Institute of Technology, and were performed in accordance with institutional and governmental guidelines.

In situ *hybridization.* Probes for *Mash1*, *Ngn1*, *NeuroD*, *SCG10*, *GAP43*, and *OMP* were prepared as previously described (Hirota and Mombaerts, 2004). Probes for $G\alpha_{i2}$, $G\alpha_o$, *V1rb1*, *V1rd16*, *V1re4*, *V2ra*, *V2rb*, and *V2rc* were provided by P. Mombaerts, Max-Planck Institute of Biophysics, Frankfort, Germany (Rodriguez et al., 2002; Ishii et al., 2003). Other probes were prepared from the cDNA of *Bcl11b* (nucleotides 1501-2560, GenBank accession number BC19503), *Vil1* (nucleotides 356-2634, NCBI reference sequence NM_009509), *Tcfap2e* (nucleotides 916-1875, NCBI reference sequence NM_198960), *Cart* (nucleotides 96-788, NCBI reference sequence NM_001081493), *Big2/Contactin4* (nucleotides 1189-2575, NCBI reference sequence NM_173004.3), *Mef2b* (nucleotides 500-1255, NCBI reference sequence NM_00445484), *Panx3* (nucleotides 165-1598, NCBI reference sequence NM_172454), *Meis2* (nucleotides 453-1354, NCBI reference sequence NM_001136072.2), and *Olig1* (nucleotides 971-1919, NCBI reference sequence NM_016968.4). Single-color and two-color *in situ* hybridization (ISH) was performed according to a method described previously (Ishii et al., 2003, 2004). For two-color ISH, tyramide signal amplification (TSA)-biotin, TSA-dinitrophenyl, and TSA-plus biotin systems (PerkinElmer) were used. The images were taken on an Olympus BX51 microscope with a DP71 digital CCD camera for bright-field images and a Leica SP or SPE confocal microscope for fluorescent images.

Immunohistochemistry. Immunohistochemistry (IHC) was performed according to a previously described method (Hirota et al., 2007). The following primary antibodies and dilutions were used: rabbit anti-Bcl11b (1:200) (Wakabayashi et al., 2003b); goat anti-Ki67 (1:1500 or 1:3000, catalog #SC-7846, Santa Cruz Biotechnology); goat anti-OMP (1:5000, catalog #544-10001, Wako); guinea pig anti-GABA (1:1000 or 1:10,000, catalog #AB175, Millipore); rabbit anti-Tbx21 (1:5000, a gift from Y. Yoshihara, RIKEN, Wako, Japan) (Yoshihara et al., 2005); guinea pig anti-Tbx21 (1:1000, a gift from Y. Yoshihara) (Yoshihara et al., 2005); mouse anti-NCAM (1:500, catalog #C-9672, Sigma); mouse anti-synaptophysin (1:1000, catalog #MAB5258, Millipore); rabbit anti-protocadherin 21 (1:1000, a gift from Dr. Yoshihara) (Kaneko-Goto et al., 2008); and rabbit anti-active caspase-3 (1:500 or 1:5000, catalog #C92–605, BD Pharmingen). The following appropriate secondary antibodies were used: the Alexa series (Invitrogen) and Cy3- and Cy5-conjugated goat anti-rabbit IgG (Jackson Immuno Research Laboratories); biotin-conjugated donkey anti-goat IgG (Rockland); biotin-conjugated goat anti-guinea pig IgG and goat anti-rabbit IgG (Vector Laboratories) antibodies. For the immunostaining that used the anti-Ki67 or anti-active caspase-3 antibodies, the sections were treated with the Vector Avidin/Biotin Blocking Kit (Vector Laboratories) and incubated with primary antibodies. Immunostaining was performed using the Vectastain Detection Kit (Vector Laboratories) in combination with the TSA-biotin system (PerkinElmer) to amplify signals. Anti-Ki67 immunoreactivity was detected using the DAB-chromogenic method with streptavidin-HRP, and anti-active caspase-3 was detected with streptoavidin-Alexa488 fluorescence. For immunostaining with the mouse anti-NCAM and anti-synaptophysin antibodies, the sections were pretreated with the Vector M.O.M. Immunodetection Kit (Vector Laboratories) before treatment with the primary antibody. For immunostaining of the nuclear protein, we performed antigen-retrieval pretreatment in 10 mM sodium citrate for 10 min or in HistoVT One (Nacalai Tesque) at 70°C for 15 min using a microwave oven.

Quantitative analyses. To quantify the number of DAPI-positive cells, *VR*-expressing cells, $G\alpha_{i2}$ and $G\alpha_o$-expressing cells, proliferating cells, and apoptotic cells, every fifth or tenth coronal section (10 μm thickness), or every third coronal section (20 μm thickness) throughout the vomeronasal organ (VNO) was collected for each staining experiment, and the number of positive cells was counted.

DiI tracing experiment. DiIC18(3) (DiI) crystal (Invitrogen) was heat melted to coat a glass capillary. After dissection of the heads of *Bcl11b*$^{-/-}$ and wild-type mice, the nose tip was cut to expose the rostral vomeronasal organ, and the DiI-coated glass capillary was placed into the lumen of the VNO. Samples were incubated in PBS for 2 h at 37°C, in 0.5% PFA/PBS overnight, and in 4% PFA/PBS for a month at room temperature to allow for the diffusion of DiI from the VSNs to the axonal termini. The DiI fluorescence of sagittally transected heads was imaged using an Olympus BX51 fluorescence microscope with a DP71-digital CCD camera.

Affymetrix microarrays. VNOs were obtained from *Bcl11b*$^{-/-}$ and wild-type mice at P0 and stored in RNA*later* (Ambion). The total RNA of each preparation was extracted using the RNeasy Mini Kit (Qiagen). Biotinylated cRNA was synthesized using 10 ng of total RNA with the Two-Cycle Target Labeling and Control Reagents Kit (Affymetrix), fragmented, and hybridized to the DNA microarrays (Mouse Genome 430 2.0 Array). To ensure reproducibility, microarray analyses were performed with RNA samples from six *Bcl11b*$^{-/-}$ and five wild-type mice. The microarray data were linearly normalized with the GAPDH (Probe ID: 1418625_s_at) signal of each preparation using GeneChip operating software (Affymetrix). The statistical significance of gene expression differences between *Bcl11b*$^{-/-}$ and wild-type was analyzed using GeneSpring version 7.3 (Agilent Technologies), and differentially expressed genes with a false discovery rate <0.25 were extracted from the data for further experiments.

Results

Bcl11b is expressed in the developing vomeronasal epithelium

The expression of *Bcl11b*/*Ctip2* has been reported in the embryonic main olfactory epithelium (MOE) (Leid et al., 2004), but its expression in the VNE has not been studied. Because the MOE and the VNE are derived from the same olfactory placode, we assumed that *Bcl11b* would also be expressed in the VNE. Therefore, we examined the expression of *Bcl11b* in the developing VNE using ISH. The ISH studies revealed that *Bcl11b* was expressed in the VNE during the course of fetal development to adulthood, and its expression levels and patterns changed dynamically (Fig. 1*A*). The expression of *Bcl11b* was observed in the vomeronasal groove/VNE, and the MOE at the earliest time point examined, E11.5, which is shortly after the olfactory pits invaginate to develop the VNE and the MOE (Cuschieri and Bannister, 1975; Garrosa et al., 1998). The expression of *Bcl11b* increased gradually in level and in the number of cells during embryogenesis (Fig. 1*A*). From E16.5 to P0, a strong expression of *Bcl11b* was detected in the VSN layer but not in the sustentacular cell layer. Expression levels in individual cells were not uniform; rather, high-, low-, and nonexpressing cells were intermingled in the embryonic VNE. After birth, *Bcl11b* expression changed dynamically: *Bcl11b* expression gradually decreased and was restricted to the marginal region of the VNE (Fig. 1*A*, arrows), where neuronal progenitor/precursor cells and immature neurons localize. This result indicates that *Bcl11b* is expressed mainly in proliferating cells and/or immature neurons. Because proliferating cells and differentiating and differentiated neurons intermingle in the VNE during embryogenesis and for several days postnatally, the differential expression levels

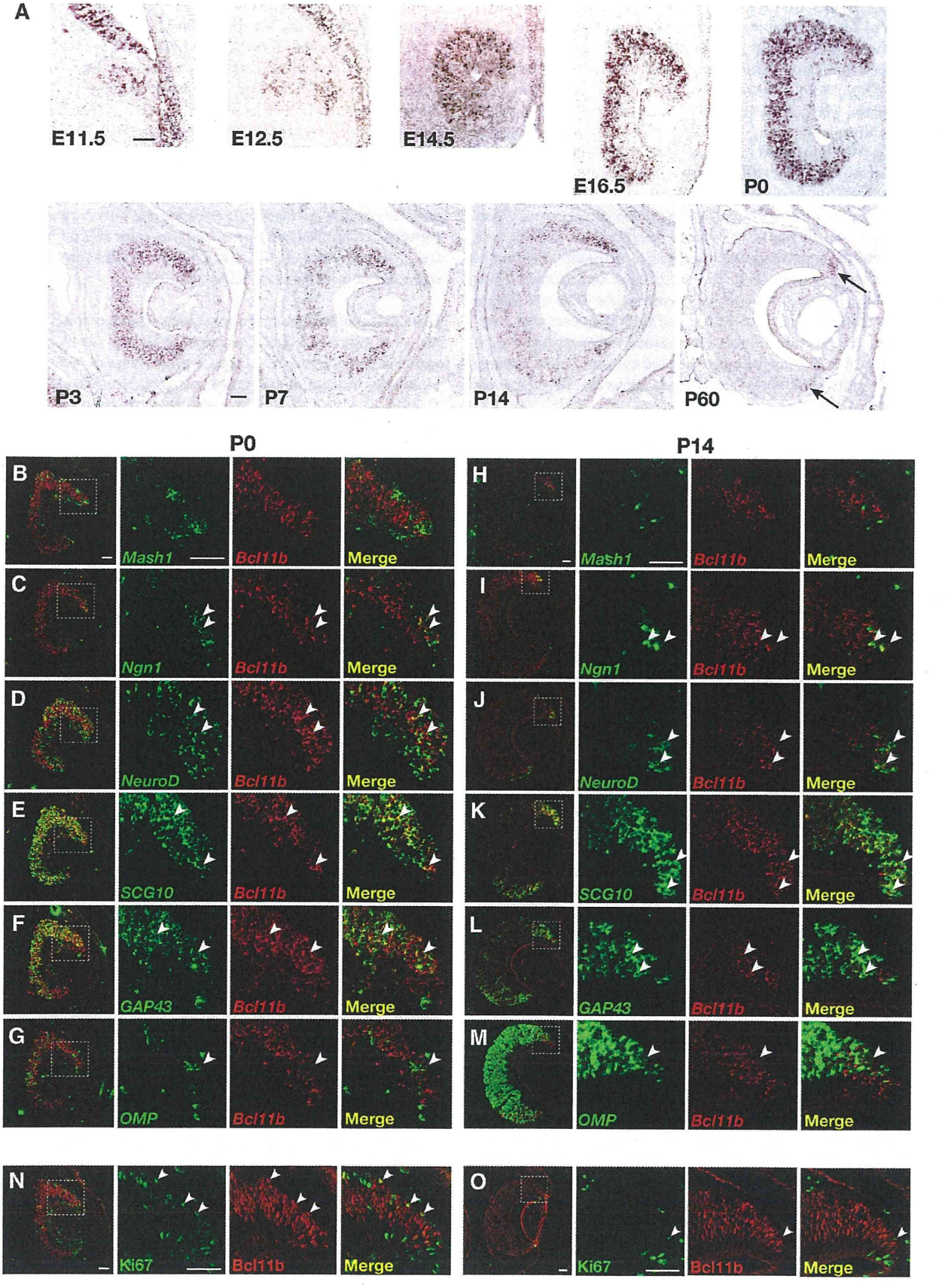

Figure 1. Expression of *Bcl11b* in the developing mouse vomeronasal epithelium. ***A***, *In situ* hybridization with RNA probes for *Bcl11b* in coronal sections of the VNE at E11.5, E12.5, E14.5, E16.5, P0, P3, P7, P14, and P60. The expression of *Bcl11b* gradually increased during embryogenesis. After birth, the expression of *Bcl11b* gradually decreased and was restricted *(Figure legend continues.)*